Absolute Measurements of mRNA Translation in *Caulobacter crescentus* Reveal Important Fitness Costs of Vitamin B$_{12}$ Scavenging

James R. Aretakis,[a] Alisa Gega,[a] Jared M. Schrader[a]

[a]Department of Biological Sciences, Wayne State University, Detroit, Michigan, USA

ABSTRACT *Caulobacter crescentus* is a model for the bacterial cell cycle which culminates in asymmetric cell division, yet little is known about the absolute levels of protein synthesis of the cellular parts needed to complete the cell cycle. Here we utilize ribosome profiling to provide absolute measurements of mRNA translation in *C. crescentus*, providing an important resource with quantitative genome-wide measurements of protein output across individual genes. Analysis of protein synthesis rates revealed ~4.5% of cellular protein synthesis is for genes related to vitamin B$_{12}$ import (*btuB*) and B$_{12}$-independent methionine biosynthesis (*metE*) when grown in common growth media lacking B$_{12}$. While its facultative B$_{12}$ lifestyle provides a fitness advantage in the absence of B$_{12}$, we find that it provides a fitness disadvantage of the cells in the presence of B$_{12}$, potentially explaining why many *Caulobacter* species have lost the *metE* gene and become obligates for B$_{12}$.

IMPORTANCE *Caulobacter crescentus* is a model system of the bacterial cell cycle culminating in asymmetric cell division, with each daughter cell inheriting a distinct set of proteins. While a genetic network of master transcription factors coordinates the cell cycle timing of transcription for nearly 20% of *Caulobacter* genes, we lack knowledge of how many of each protein "part" encoded in the genome are synthesized. Therefore, to determine the absolute production rates across the genome, we performed ribosome profiling, providing, for the first time, a quantitative resource with measurements of each protein "part" needed to generate daughter cells. This resource furthers the goal of a systems-level understanding of the genetic network controlling asymmetric cell division. To highlight the utility of this data set, we probe the protein synthesis cost of a B$_{12}$ utilization pathway and provide new insights into *Caulobacter*'s adaptation to its natural environments.

KEYWORDS absolute quantitation, *Caulobacter crescentus*, ribosome profiling, vitamin B$_{12}$, cell cycle

In bacterial systems biology, global mRNA translation measurements are critical for understanding how cells utilize their resources to achieve their evolutionarily selected cell growth and division cycles. To complete the bacterial cell cycle, the protein parts encoded within the genome must be transcribed into mRNAs that are translated into the appropriate number of proteins for the daughter cells to be generated. Genome-wide absolute quantitation of protein level measurements has allowed the monitoring of protein resource allocation (1, 2), revealing that these cells allocate resources for optimal growth. As the ribosome content is positively correlated with the growth rate (3), cells must optimize the fraction of protein synthesis needed to make new ribosomes (enzymes that make proteins) versus the protein synthesis needed to produce the proteomes of the daughter cells to achieve short generation times (2, 4). Optimality has also been observed at the protein-complex level, as translation of a stoichiometric

amount of protein subunits to the overall multiprotein complexes has been observed (2), with different posttranscriptional strategies across species utilized to achieve the optimal protein concentration (5). Therefore, to understand the mechanisms controlling the growth and division cycles of diverse bacteria, we must understand how bacteria are able to optimize their protein synthesis resources for maximal fitness.

Caulobacter crescentus is an oligotrophic alphaproteobacterium with a carefully orchestrated cell cycle yielding asymmetric cell division and a model organism for the study of the bacterial cell cycle (6, 7). In *C. crescentus*, cells undergo changes in gene expression of ~20% of their entire genome during the process of the cell cycle (8, 9). Timing of 57% of the cell cycle-regulated mRNAs is controlled at the transcription level by a master regulatory circuit that is composed of 4 transcription factors (DnaA, GcrA, CtrA, and SciP) and a DNA methylase (CcrM) (6, 10), and 49% of those cell cycle-regulated mRNAs are additionally regulated at the level of mRNA translation (8). Importantly, global *C. crescentus* studies have focused solely on the control of the timing of gene expression in the cell cycle, and thus, little is known about the absolute levels of protein synthesis, or how the protein synthesis resources are allocated across the proteome.

Here, we utilize ribosome profiling to achieve a quantitative genome-wide absolute measure of protein synthesis in *C. crescentus*. This resource provides the absolute protein synthesis rate of each protein expressed from the *C. crescentus* genome and a global map of protein synthesis resource allocation. Absolute levels of mRNA translation of cell cycle master regulators showed higher levels of mRNA translation compared to their known DNA binding sites for all but CcrM and a relatively low level of mRNA translation of CtrA regulatory proteins relative to the CtrA master regulator itself. PopZ, a polar protein scaffold that recruits asymmetric cell fate specification proteins (11), is at a limiting concentration compared to its client proteins, suggesting that these clients compete for access to the cell pole. Surprisingly, we discovered that the *btuB* vitamin B_{12} importer and the *metE* methionine-biosynthetic gene were among the most highly translated genes in the absence of B_{12}, showing that the *C. crescentus* B_{12}-scavenging pathway requires a surprisingly large amount of the cell's protein synthesis resources. The high cost of protein synthesis of the B_{12}-scavenging pathway is reduced in the presence of B_{12} by riboswitches in the 5' untranslated region (UTR) of these two genes. The widely utilized lab strain NA1000 is a facultative B_{12} scavenger due to the *metE* gene, which produces methionine in the absence of B_{12}, yet many natural *Caulobacter* isolates are obligate B_{12} scavengers (12). We show that the facultative B_{12}-scavenging lifestyle generates a fitness tradeoff, where in the absence of B_{12} there is a positive fitness advantage from MetE's B_{12}-independent methionine production, while in B_{12}'s presence there is a fitness disadvantage due to the wasted cost of MetE's protein synthesis, providing an explanation for why many isolates have lost the *metE* gene to become obligates for B_{12}.

RESULTS

Absolute quantitation of mRNA translation rates. Ribosome profiling provides a global direct measure of the protein synthesis rate by sequencing ribosome-protected mRNA footprints (2, 13, 14). To determine absolute rates of translation in *C. crescentus*, ribosome profiling was performed in unsynchronized *C. crescentus* NA1000 cells grown in M2G minimal medium. In fast-growing bacteria where the rate of translation is the main driving force of protein levels, protein degradation can be negligible, and therefore, the main driving force of protein levels is mRNA translation (2). This is largely true in *C. crescentus*, as >95% of proteins were found to have half-lives longer than the cell cycle (15). First, we examined the ribosome footprint density along each open reading frame (ORF) on mRNAs as a relative measure for translation (Fig. 1A). For example, in the *divK/pleD* polycistronic operon, we find that *divK* has 2.0-fold-higher ribosome density than *pleD* (Fig. 1A). For absolute quantitation, it is assumed that the average elongation rate is constant for each mRNA, which would allow the average ribosome density to be directly proportional to the rate of protein synthesis of each
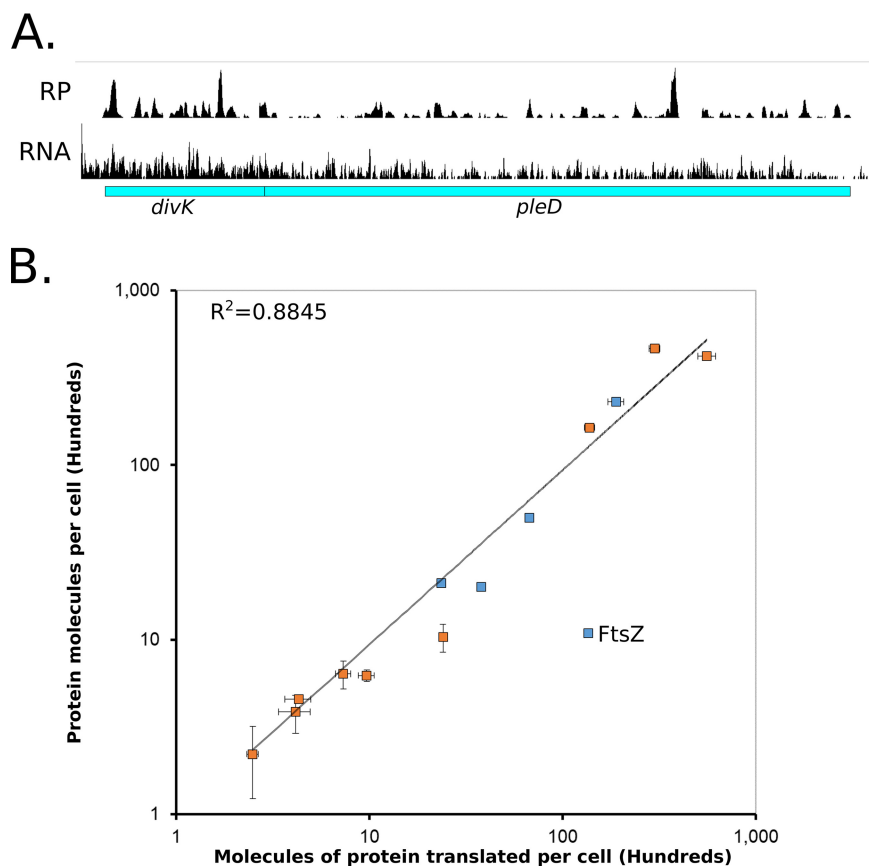
FIG 1 Absolute quantitation of *C. crescentus* protein synthesis by ribosome profiling. (A) Ribosome profiling data for cells grown in M2G medium of the *divK/pleD* operon. Average ribosome density of *divK* is 2.0 times higher than for *pleD*. mRNA data are from reference 36. (B) Absolute protein levels of unsynchronized cells measured by Western blotting (blue) or YFP fusions (orange) compared to the absolute molecules of protein translated per cell calculated by ribosome profiling. Vertical error bars indicate the standard deviation in YFP intensity or standard deviation for the Western blots, while horizontal error bars indicate the standard deviation from ribosome profiling replicates (*n* = 3). FtsZ is expected to deviate from the line since its protein levels are under proteolytic control (17). Data are in Tables S1 and S2.

ORF (2). It is also assumed that all ribosomes will finish translation and make the full-length protein (2). Next, to reduce the impact of fast- and slow-moving ribosomes in the ribosome occupancy profiles along ORFs on the quantitative level of translation, we used winsorization to correct the average ribosome footprint density of each ORF (see Table S1 in the supplemental material). Start codon and stop codon regions were omitted from the analysis to avoid biases in slow-moving ribosomes that are initiating or terminating (13, 16).

To convert ribosome density to absolute mRNA translation rates, we measured the average protein mass of *C. crescentus* cells, which was multiplied by the fractional ribosome density measurement of each gene and divided by the molecular weight ($k_i = \phi_i P/mW_i$) (2). This measure of the average number of proteins translated per cell correlated well between the protein concentrations reported in the literature as well as protein concentration measurements reported here using yellow fluorescent protein (YFP) intensity of C-terminally tagged gene fusions (Fig. 1B; Fig. S1 and Table S2). As expected, FtsZ, the key cell division protein which is known to be a substrate of cell cycle-dependent proteolysis (17), has a 13-fold-larger amount of translated protein than protein observed in the cell, while stable proteins ranged between 0.65- and 2.3-fold. The same phenomenon of higher translation levels than protein levels was also observed for the proteolyzed cell cycle regulators DnaA and CcrM, and upon deletion of the Lon protease, which is known to be responsible for their proteolysis, the

correlation was restored (Peter Chien, personal communication) (Fig. S1) (18, 19). These data suggest that the absolute measures of mRNA translation are reflecting the absolute protein synthesis rate for each ORF in *C. crescentus* and provide a reasonable measure of steady-state protein levels for stable proteins (data can be found in Table S1).

Global analysis of *C. crescentus* absolute mRNA translation levels. *C. crescentus* cells dedicate a significant percentage of their protein synthesis to several major cellular processes associated with cell growth (Fig. 2A; Fig. S2). Across major KEGG categories, we analyzed the percentage of ribosome footprints to understand their allocation of protein synthesis capacity (Table S3). Nutrient transporters (11.8%), the ribosome (11.2%), and the cell envelope (9.8%) represent the largest classes of protein production for *C. crescentus*. A significant fraction of protein synthesis capacity (25.5%) is allocated to produce proteins of unknown function, showing that a significant fraction of the cell's protein synthesis capacity is not understood. By comparing the fraction of the translation KEGG category across minimal medium (M2G) (15.9%) and a richer complex medium (peptone-yeast extract [PYE]) (22.8%), we find that the cells dedicate a larger amount of protein synthesis capacity to making translational machinery in rich medium, similar to *Escherichia coli* (3). Additionally, we see that a larger amount of protein synthesis capacity in "cell growth and death" is observed in M2G (11.3%) than in PYE (6.45%), owing largely to increased protein synthesis capacity of an operon of cell-contact-dependent toxins and immunity proteins that are known to be expressed in stationary phase (Fig. S2) (20).

Interestingly, while the cell cycle is a major area of study in *C. crescentus*, the cell cycle genes represent only a small fraction of protein synthesis capacity (1.78%), and yet these genes play a critical role in shaping the growth and division cycles. The cell cycle-regulatory circuit itself is composed of four transcription factors (DnaA, GcrA, CtrA, and SciP) and a DNA methylase (CcrM) whose spatiotemporal activation facilitates cell cycle progression (6). For master regulator proteins, the cell produces between ~3,000 and 30,000 copies of each protein, which corresponds to between 71- and 648-fold more proteins than the number of known DNA binding sites that they control (10), with the exception of CcrM (Table S4). Three thousand two hundred eighty CcrM proteins are translated to methylate the 4,542 GANTC sites per chromosome (Fig. 2B). While the number of CcrM proteins is approximately one-third the number of GANTC sites present after DNA replication, CcrM is a processive enzyme (21), suggesting that each CcrM may on average methylate ~3 GANTC sites. While the number of CtrA proteins translated (25,400 proteins) corresponds closely with the amount measured in predivisional cells (18,000 to 22,000 [22, 23]), CtrA is produced at a significantly higher level than its collection of regulatory kinases, phosphotransferases, and proteolytic adapters that control its cell cycle-dependent activity (Fig. 2B). GcrA interacts with the RNA polymerase/σ^{70} complex to activate transcription of target promoters (24), where an ~4-fold excess of GcrA over σ^{70} is produced, suggesting that excess GcrA may accelerate binding to the RNA polymerase holoenzyme (25) to facilitate subsequent recruitment of σ^{70}.

As many proteins were found to have distinct subcellular patterns of protein accumulation in *C. crescentus* as determined in reference 26, we compared protein synthesis capacity to the localization patterns of proteins observed in this data set (Fig. 2C). Seven percent of protein synthesis occurs for "localized proteins" in *C. crescentus*. Of those localized proteins, most are "patchy/spotty," while a significant fraction has a subcellular address where the protein accumulates (pole, stalk, or center) (Fig. 2C). Many proteins are specifically required to form asymmetric polar protein complexes that function to determine cell fate upon division (6). Many of these polarly localized proteins are recruited to the cell pole through the multimeric hub protein PopZ (27–29). Interestingly, by examining PopZ and its known client proteins, we find that PopZ is made in limiting amounts (Fig. 2D), suggesting that the clients compete for PopZ binding *in vivo*.
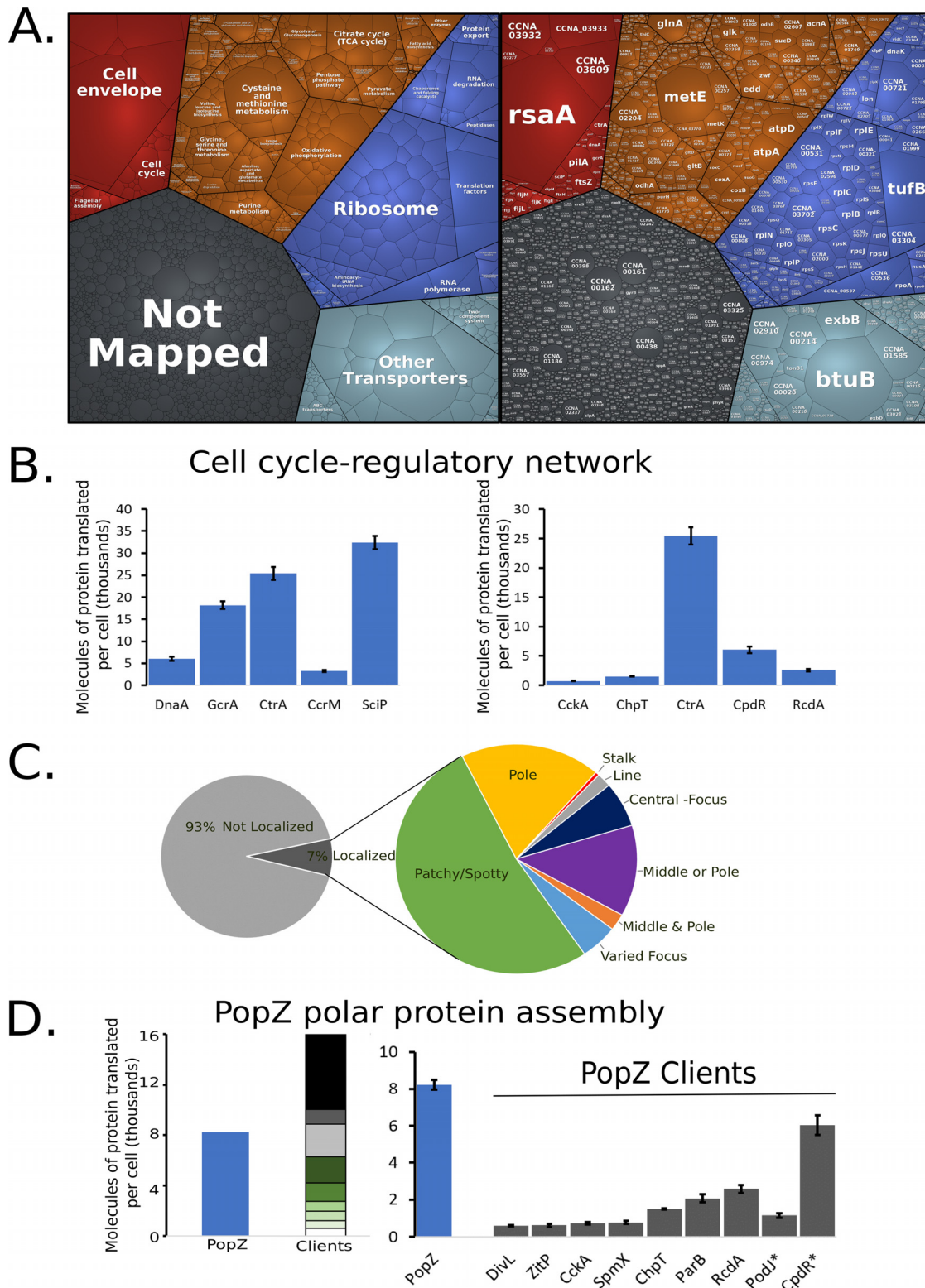
FIG 2 Global analysis of *C. crescentus* protein synthesis. (A) Proteomap with each polygon representing a single gene with area scaled to the fraction of ribosome-protected mRNA footprints measured. Red is cellular processes, orange is metabolism, blue is genetic information processing, light blue is environmental information processing, and gray is genes of unknown function. (B) Molecules of protein translated per cell for the cell cycle master regulators (left) and CtrA regulatory network (right). (C) (Left) Fraction of ribosome-protected mRNA footprints encoding localized (dark gray) or nonlocalized (light gray) proteins. (Right) Zoomed-in analysis of the fraction of proteins with different subcellular localization patterns based on reference 26. (D) Polar protein competition. (Left) Molecules of protein translated per cell for the polar protein scaffold PopZ and its known clients (27–29). Proteins with known proteolysis are highlighted with asterisks.

Analysis of vitamin B$_{12}$ and methionine metabolism. Analysis of the most highly translated proteins found that RsaA, the surface layer protein, was the most highly translated protein in the cell (Fig. 3A) (30). Elongation factor Tu was the third most abundant cytoplasmic protein owing to its requirement to deliver aminoacyl-tRNAs to the ribosome during translation (31). Surprisingly, we also observed that the homolog of the B$_{12}$ importer (*btuB*, second highest) and the methionine-biosynthetic gene (*metE*, fourth highest) were among the most highly translated proteins. Vitamin B$_{12}$ is an important enzymatic cofactor that in *C. crescentus* is used for the biosynthesis of methionine, deoxynucleoside triphosphate (dNTP) production, tRNA modification, and isomerization of methylmalonyl coenzyme A (CoA) to succinyl-CoA (Fig. 3) (32). *C. crescentus* cannot synthesize B$_{12}$ *de novo* but can import it through the BtuB protein (33). In the cytoplasm, both MetE and MetH perform the rate-limiting step of methionine biosynthesis, where MetH requires B$_{12}$ but has a higher specific activity than MetE (Fig. 3B) (34, 35). Of note, both BtuB and MetE are translated at much higher levels than the other components related to methionine biosynthesis (Fig. 3B). Both the *btuB* and *metE* genes are the only two genes in *C. crescentus* with B$_{12}$ riboswitches encoded in their 5′ UTRs (36). We tested the function of these riboswitches by creating 5′ UTR fusions to the mCherry gene driven by the vanillate promoter and subjecting the cells to various concentrations of B$_{12}$ in the form of cyanocobalamin (Fig. 3C). Both the *metE* and *btuB* 5′ UTR reporters showed high translation in the absence of B$_{12}$ and exhibited a B$_{12}$ concentration-dependent translational shutoff (Fig. 3C). The *metE* riboswitch appears to be more sensitive to B$_{12}$ concentration, with a $K_{1/2}$ of 0.062 nM, while the *btuB* riboswitch $K_{1/2}$ was 0.19 nM, both in line with the concentrations found in aquatic ecosystems (Fig. S3) (37, 38). Taken together, these data show that *C. crescentus* cells are investing a large amount of their protein synthesis capacity toward B$_{12}$ uptake and the B$_{12}$-independent methionine pathway in the absence of B$_{12}$. We therefore hypothesized that the cells are wasting energy in the absence of B$_{12}$ by producing these very costly proteins.

To assess if the cells are wasting energy from the B$_{12}$-related pathways, we examined the fitness of *C. crescentus* cells with disruptions in the nonessential components of these pathways in the absence of B$_{12}$ (Fig. 4A). For this, we used published transposon sequencing (Tn-seq) data sets (39) and analyzed B$_{12}$-related genes whose disruption would not have polarity effects (single genes or last genes in operons) in M2G minimal medium or PYE rich medium, neither of which contains B$_{12}$ (12, 40). In M2G minimal medium, cells require the *metE* gene to make methionine (33), while the other nonessential B$_{12}$-related components showed increases in fitness when disrupted that were proportional to their protein synthesis costs (Fig. 4A). In PYE rich medium, which contains methionine in the peptone, the *metE* gene is no longer essential, but instead, its disruption leads to higher fitness (39). Indeed, all the components of the methionine pathway led to increases in fitness proportional to their protein synthesis cost when disrupted in PYE (Fig. 4A) (39). These data show that in the absence of B$_{12}$, the excessive translation of these proteins leads to unnecessary costs of protein synthesis that limit the fitness of *C. crescentus* cells.

To test the effects of B$_{12}$ on *C. crescentus* cell growth, we examined the growth rate of cells cultured in M2G medium containing B$_{12}$ in the form of cyanocobalamin. Here, we observe faster growth in a B$_{12}$ concentration-dependent manner (Fig. 4B; Table S5), with up to a 21% faster doubling time observed at 1 nM B$_{12}$ in M2G medium. Eleven percent acceleration of cell growth rates also occurs in PYE medium, which contains methionine in the peptone, suggesting that the growth enhancement of B$_{12}$ is likely caused in part by reduced protein synthesis costs from *btuB* and *metE* riboswitches. We attempted to separate B$_{12}$'s effects on methionine synthesis from its effects on other pathways by addition of exogenous methionine in the presence or absence of B$_{12}$, but exogenous methionine leads to a dramatic decrease in growth by an unknown mechanism (41). Overall, we find that B$_{12}$ significantly enhances the growth rate of NA1000 cells.
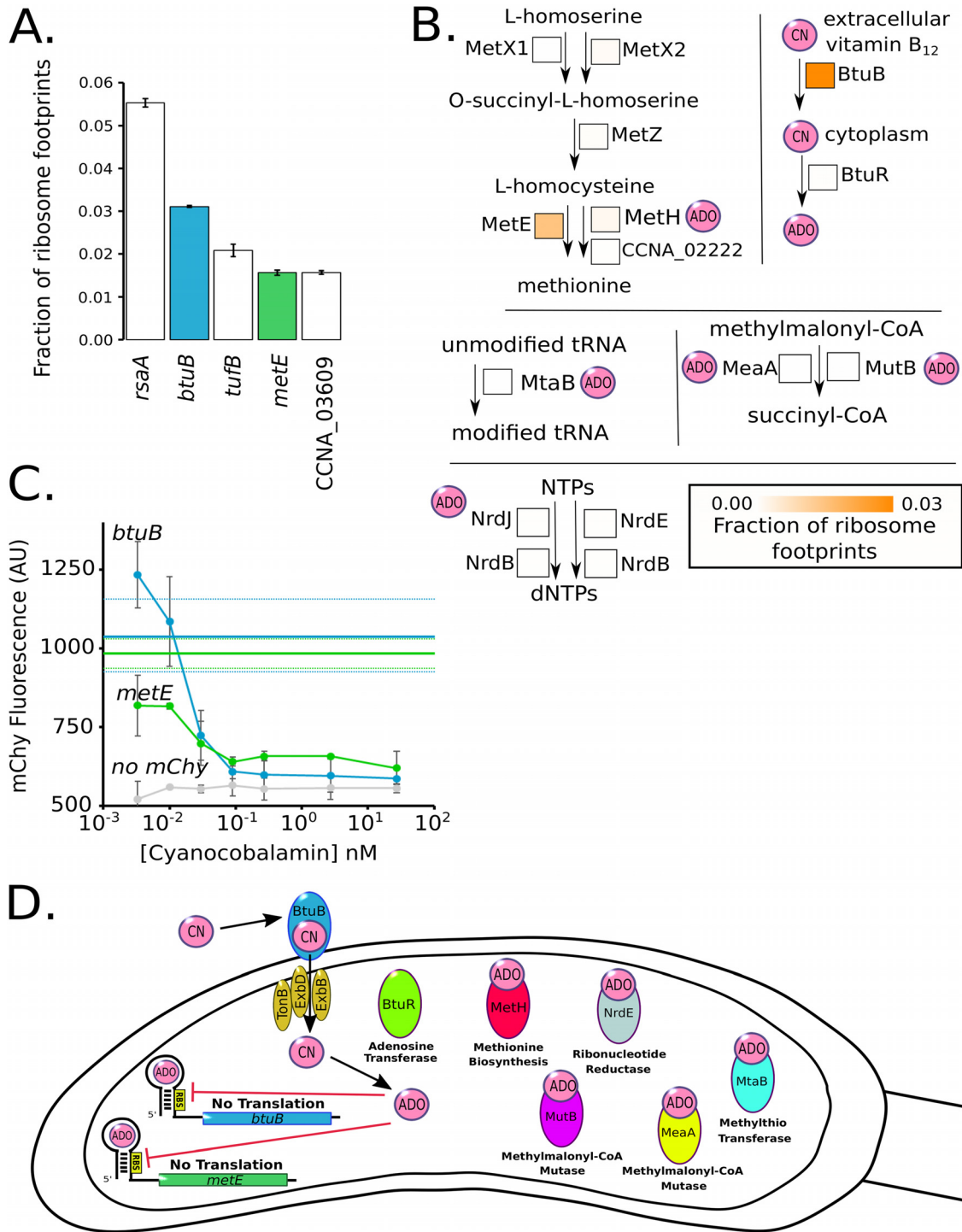
FIG 3 *C. crescentus* cells are starved for B_{12} in laboratory growth medium. (A) Fraction of ribosome footprints for the most highly translated mRNAs in M2G. B_{12}-related genes are colored. (B) Pathway of methionine biosynthesis, MetX1 (CCNA_03309), MetX2 (CCNA_00559), MetZ (CCNA_02321), MetE (CCNA_00515), MetH (CCNA_02221), and CCNA_02222. Pathway for B_{12} utilization, BtuB (CCNA_01826) and BtuR (CCNA_02321). Pathway for tRNA modification, MtaB (CCNA_03798). Pathway for nucleotide reduction, NrdJ (CCNA_01966), NrdE (CCNA_03607), and NrdB (CCNA_00261). Pathway for succinyl-CoA biosynthesis, MeaA (CCNA_03177) and MutB (CCNA_02459). Square boxes next to each enzyme contain an orange heat map which represents the fraction of ribosome footprints. ADO (adenosyl) and CN (cyano) refer to the B_{12} upper ligand. (C) Negative regulation by B_{12} riboswitches on the *btuB* and *metE* genes. Translation reporters for the *btuB* and *metE* genes fused to mCherry assayed in M2G with the indicated concentrations of B_{12}. Error bars represent standard deviation for mCherry fluorescence in three biological replicates of the B_{12} dilution series ($n = 3$). Solid blue and green horizontal lines indicate the mChy fluorescence without vitamin B_{12} for *btuB* and *metE*, respectively, and dashed lines indicate the standard deviation. (D) Cartoon of B_{12}-regulated pathways in *C. crescentus*. *btuB* and *metE* genes contain negative regulatory B_{12} riboswitches. BtuB and BtuR are part of the B_{12} import and utilization pathway. MetH, NrdE, MeaA, MutB, and MtaB are B_{12}-dependent enzymes for methionine biosynthesis.
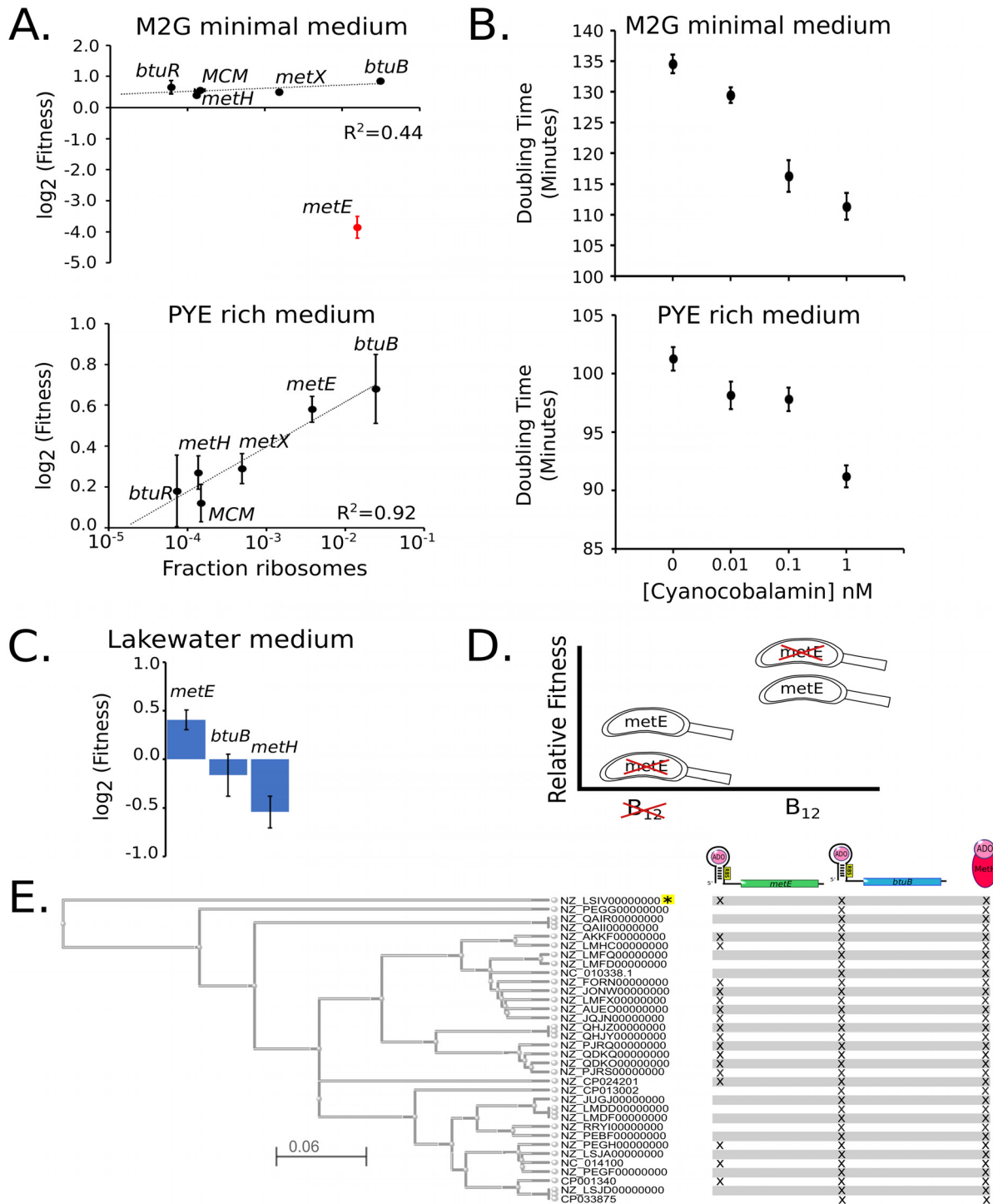
FIG 4 Excess protein synthesis rates for methionine-biosynthetic genes correlate with fitness cost. (A) Protein synthesis cost measured in the fraction of ribosomes (Table S1) on the x axis versus the Tn-seq-derived fitness values for the btuB B_{12} importer and methionine-biosynthetic genes under growth in minimal or rich medium as measured previously (39) (biological replicates, $n = 2$ for M2G, $n = 10$ for PYE). Black points represent nonessential genes for methionine biosynthesis, and red points represent genes required for methionine biosynthesis under the specified growth condition. Error bars represent standard deviation. Curve fits were performed only on nonessential genes. (B) Doubling times of *C. crescentus* cells in M2G and PYE media with indicated concentrations of B_{12}. Error bars represent the standard deviation for doubling time measurements (biological replicates, $n = 3$ for each condition). (C) Tn-seq-derived fitness values for metE, btuB, and metH under growth in Lake Michigan lake water as measured previously (57). (D) Fitness tradeoff of facultative versus obligate B_{12} scavenging. Relative fitness shown for species with metE (facultative) or without metE (obligate) in environments lacking or containing sufficient B_{12}. (E) Phylogenetic tree of all *Caulobacter* species with completed genomes based on btuB and metH protein sequences. Each species is labeled by its NCBI accession identifier, and the scale represents the Kimura distance. Marks next to species represent the presence of a metE, btuB, or metH gene. All species have a predicted B_{12} riboswitch upstream of btuB and metE genes (not shown), except the species noted with the yellow asterisk. A list of species names can be found in Table S7.

DISCUSSION

Absolute quantitation of protein synthesis in *C. crescentus*. As the cost of protein synthesis is a significant output of the cell's energy, absolute quantitation of translation is a powerful method to measure gene expression and resource allocation. Here, we present an absolute protein synthesis resource for *C. crescentus* generated by ribosome profiling which will be vital for systems modeling efforts for the *C. crescentus* cell cycle (42–45) and in the subsequent optimization of synthetic *Caulobacter* genomes (46, 47). Across the proteome, the mRNA translation resource allocation showed that 1.4% of the translation machinery is dedicated to translation of cell cycle-regulatory genes. We observed that for all the cell cycle master regulators, except CcrM, the number of proteins translated dramatically exceeds the total number of DNA binding sites in the genome (Fig. 2B). We hypothesize that the high concentrations of these factors may facilitate rapid activation of target gene transcription during each phase of the cell cycle.

Approximately 7% of protein synthesis capacity is dedicated to genes whose protein products were found to be localized in one of several modes of subcellular organization (Fig. 2C) (26). Recent reports suggest that some of these foci are formed by liquid-liquid phase separation of the proteins into membraneless organelles (48, 49). For *C. crescentus* BR bodies, the concentration of the condensate-forming protein RNase E (6.3 μM) appears to correspond closely to the transition boundary for liquid-liquid phase separation (48), potentially allowing control of the assembly of these bodies. Interestingly, we observed that the polar protein scaffold PopZ, which facilitates recruitment of asymmetrically localized signaling proteins to the cell poles (11, 27, 29), is present at approximately one-half the concentration of its client proteins, suggesting that clients compete for PopZ access (Fig. 2D). Dynamic competition of clients for PopZ may be important for the ordered assembly of unique proteins at each cell pole and may impact the spatial activation of downstream signaling outputs (27, 50, 51).

Implications of B$_{12}$-scavenging pathway for environmental fitness. B$_{12}$ is an important enzymatic cofactor that is required for the activity of enzymes involved in biosynthesis of methionine, dNTP production, tRNA modification, and isomerization of methylmalonyl-CoA to succinyl-CoA (Fig. 3B and D) (32). Like many bacteria, *C. crescentus* cannot produce B$_{12}$ but can scavenge it from the environment (33), where it can increase the growth rate of *C. crescentus* by up to 21% (Fig. 4B). *btuB*, the B$_{12}$ importer, and *metE*, the B$_{12}$-independent methionine synthase, are among the most highly expressed genes, accounting for ~4.5% of all protein synthesis capacity (Fig. 3A). To counteract the protein synthesis demand, *btuB* and *metE* genes also contain B$_{12}$ riboswitches that reduce translation when sufficient B$_{12}$ enters the cytoplasm (Fig. 3C). Freshwater bodies typically have B$_{12}$ concentrations in the range from 0.11 nM to below the level of detection (<0.1 pM) (37, 38, 52–55), suggesting that high levels of BtuB may help facilitate import. Importantly, the conserved *metE* and *btuB* riboswitches are sensitive to B$_{12}$ in physiologically relevant ranges ($K_{1/2}$ = 0.062 nM and 0.19 nM, respectively), and their different sensitivities suggest that *metE* translation would be downregulated before shutting off the *btuB* importer. At high concentrations of B$_{12}$ that saturate the riboswitches (Fig. 4B), a significant portion of the increase in growth rate is likely due to the liberation of protein synthesis resources on these two highly expressed genes (Fig. 3A and C). When grown in M2G or PYE medium lacking B$_{12}$, disrupting the *btuB* gene increases fitness by freeing up wasted protein synthesis resources (Fig. 4A) (39). Similarly, *metE* disruption leads to increased fitness in PYE, which contains methionine, but *metE* disruption becomes essential in M2G minimal medium as it is required to make methionine (Fig. 4A) (39). Why then does *C. crescentus* have a facultative B$_{12}$ lifestyle containing both B$_{12}$-dependent and -independent methionine biosynthesis pathways?

Perhaps B$_{12}$-independent and B$_{12}$-dependent pathways exist to buffer fluctuations in environmental B$_{12}$ concentrations. The concentration of available B$_{12}$ in a freshwater body shows variation of up to 40-fold between different sampling locations and at the

same sampling location at different times (38, 52–56). Having both methionine bio-synthesis pathways adds flexibility to generate methionine under either high- or low-B_{12} conditions; however, these pathways have different protein synthesis costs. The B_{12}-independent pathway requires 1.57% of the total protein synthesis capacity to make sufficient MetE, while the B_{12}-dependent MetH pathway uses only 0.156% (Fig. 3B). Interestingly, disrupting the *metE* gene in lake water leads to a fitness advantage; however, disrupting *btuB* or *metH* leads to a fitness decrease as determined in reference 57 (Fig. 4C). Although not measured directly, the gene fitness signature from the experiment leads us to infer that physiologically relevant B_{12} concentrations were present in the sampled lake water (57). The increased fitness of *metE* disruptions in lake water suggests that increased biosynthetic flexibility comes with a negative fitness cost from protein synthesis resources wasted on MetE (Fig. 4D). Forty-seven percent of fully sequenced *Caulobacter* species have lost the *metE* gene but not the *btuB* and *metH* genes, suggesting that the observed environmental fluctuations in B_{12} concentration (38, 52) alter the selective pressure on *metE* (Fig. 4E).

Surprisingly, a recent survey of available metagenomic 16S rRNA sequencing data showed that *Caulobacter* is more abundant in soil/compost than in aquatic ecosystems (58). Soil has been shown to have B_{12} levels that can range from 20 nM to 0.3 nM, correlated with levels of organic matter (59), while bodies of freshwater typically have B_{12} concentrations in the range of 0.11 nM to below the level of detection (0.1 pM) (37, 38, 53–56). The higher B_{12} concentration in soil will enhance the growth rate and may explain the increase in relative abundance in this environment.

MATERIALS AND METHODS

Bacterial strains and cell growth. A list of all bacterial strains used here can be found in Table S6 in the supplemental material (76–81). *C. crescentus* cells were grown in M2G or PYE growth medium (40) and supplemented with the appropriate antibiotic concentrations (60). *E. coli* cells used for cloning were grown in LB medium and supplemented with the appropriate antibiotics.

Ribosome profiling. Ribosome profiling was performed similarly to procedures in references 8 and 36, except that contaminating rRNA fragments generated during micrococcal nuclease (MNase) digestion were depleted to allow deeper quantitation of resulting mRNA translation similarly to reference 2. For a detailed protocol for the procedure, see reference 16. Five hundred milliliters of NA1000 cells were grown in M2G medium to an OD_{600} of 0.5, treated with 100 μg/ml chloramphenicol for 2 min, and then harvested by centrifugation and flash-frozen in liquid nitrogen. Cells were then lysed on a mixer mill (Retsch mm400) for 6 cycles of 3 min at 15 Hz and thawed, membranes were pelleted, and the supernatant was footprinted by addition of MNase (Roche). After footprinting, MNase was quenched with EGTA, and samples were separated by sucrose gradient fractionation. 70S peaks were purified, phenol chloroform extracted, and ethanol precipitated (16). Resulting mRNA fragments were size selected by 10% acrylamide-1$\times$ TBE-7 M urea PAGE, end repaired, 3' adapter ligated, reverse transcribed, circular-ized, and depleted of rRNA fragments (2, 14, 16). rRNA cDNA fragments were removed using biotin-linked DNA oligonucleotides (oCaulo1, 5'/5Biosg/CGCTTACGGGGCTATCACCCA; oCaulo2, 5'/5Biosg/TGGCAACT AATCACGAGGGTT; oCaulo3, 5'/5Biosg/CTCATCTGGTTGCCCAAAAGA; oCaulo4, 5'/5Biosg/TGGTTCAGGAA TATTCACCTG) and MyOne streptavidin C1 Dynabeads (Invitrogen) as in reference 2. Resulting circular cDNAs were amplified by PCR using Phusion DNA polymerase (Fermentas) with indexing primers (61), pooled, and sequenced on an Illumina HiSeq 2000. Data for three ribosome profiling replicates were deposited in the Gene Expression Omnibus under accession number GSE126485. The three M2G replicates were further analyzed together with a PYE data set collected previously (36).

Ribosome footprint reads were mapped to the genome as center-weighted reads (13), and extremely fast and slow codons were corrected for by winsorization of the bottom 5% and top 95% of nucleotides, respectively. The resulting fraction of ribosome footprints (ϕ_i) of each gene (*i*) compared to the total ribosome footprint total was calculated and converted into the number of molecules of protein translated per cell (k_i) by the equation $k_i = \phi_i P/mW_i$, where P is the average protein mass per cell and mW_i is the protein product's molecular weight as originally described in reference 2. Average protein mass per cell (P) was measured as follows. Five-milliliter mid-log cultures of NA1000 cells were grown in M2G or PYE medium overnight in a roller wheel at 28°C. Once the cells reached an OD_{600} of 0.3, a 100-μl aliquot of the cells was diluted and counted on PYE plates to measure the number of viable cells and another aliquot was saved for protein concentration measurements. To measure protein content, 100 μl cells was spun down in a microcentrifuge at 14,000 rpm for 30 s, the supernatant was removed, and the remaining cell pellets were resuspended in 100 μl of 1$\times$ Laemmli sample buffer lacking any dyes. After resuspension, samples were boiled for 5 min at 95°C and then placed on ice. Lysate protein concentra-tions were measured using the Pierce 660-nm protein assay (Thermo Fisher) and with comparison of the lysate A_{600} with a linear curve fit of bovine serum albumin (BSA) standards. The mass of protein from the sample was then divided by the number of viable cells to yield the average protein mass/cell. The

resulting average protein masses per cell were $(492 \pm 170) \times 10^{-15}$ g/cell in M2G and $(519 \pm 228) \times 10^{-15}$ g/cell in PYE.

Absolute quantitation of C-terminal YFP fusions. Five-milliliter mid-log cultures of NA1000 cells harboring C-terminal eYFP fusions (gift of the Shapiro Lab, Stanford University) were grown in M2G or PYE medium overnight in a roller wheel at 28°C. Once the cells reached an OD_{600} of 0.3, cells were spotted on M2G agarose pads for imaging. Images were collected on a Leica DM6000B microscope with a Hamamatsu C9100 electron multiplying charge-coupled device (EMCCD) camera and a 100× PH3 Plan Apo 1.40-numerical-aperture (NA) objective with in a Semrock model 2427A YFP filter cube with 100-ms exposure time. Fluorescence intensity was quantified using ImageJ by segmenting the cells and measuring the average pixel intensity of the cell area. Background intensity was subtracted using the NA1000 average YFP pixel intensity. For each fusion strain, a minimum of 50 cells were used for the analysis with a minimum of two technical replicates. As MipZ molecules per cell had been previously measured (62) by quantitative Western blotting, we converted the MipZ-YFP pixel intensity to the number of molecules/cell and multiplied this conversion factor by the YFP intensities of all other C-terminal YFP fusions. The average across replicates and the standard deviation (σ) are reported in Table S2.

Doubling time measurements. Treatments were started from log-phase cultures grown overnight in the absence of cyanocobalamin (Sigma-Aldrich) and diluted in fresh medium to an OD_{600} of 0.05. Each treatment was split into a separate flask, and the correct amount of cyanocobalamin was added to the concentrations of 1 nM, 0.1 nM, 0.01 nM, and 0 nM. Fifty milliliters from each treatment was added to three different 250-ml Kimex flasks, for three replicates of each of the four treatments. An initial OD_{600} measurement was taken of each replicate using a cuvette and a NanoDrop spectrophotometer. The 12 250-ml flasks were then placed in a 28°C shaker incubator at 250 rpm. OD_{600} time points of each flask were taken throughout the logarithmic growth phase. An exponential regression of the log-phase time points was used to calculate the doubling time of each replicate.

Translation reporter assay. JS417, JS423, and JS440 strains were started from log-phase cultures grown overnight in the absence of cyanocobalamin and diluted in medium with vanillate and antibiotic to an OD_{600} of 0.05. A dilution series of each strain was used to fill tubes with 2 ml of culture at each cyanocobalamin concentration: 27 nM, 2.7 nM, 0.9 nM, 0.3 nM, 0.1 nM, 0.033 nM, and 0 nM. The 21 2-ml-cultures were then grown and induced over an 8-h period by placing the tubes in a 28°C shaker incubator at 250 rpm for 8 h. After 8 h, 2 μl from each culture was pipetted onto an M2G-agarose pad on a microscope slide. Each treatment was imaged on a microscope using both phase contrast and an mChy filter cube. Average fluorescent intensities were calculated using MicrobeJ (63) across a minimum of 100 cells.

B$_{12}$ homolog identification and phylogenetic tree mapping. Protein sequences for *btuB*, *metH*, and *metE* were determined for each *Caulobacter* species with a complete genome by using the NCBI Basic Local Alignment Search Tool (BLAST) with default settings by searching the protein sequence of each NA1000 gene for homologs with an E score of $<10^{-19}$ (64). The *btuB* and *metH* genes were then used to generate the phylogenetic tree using the NCBI Genome Workbench software and the MUSCLE multiple sequence alignment package (65). The tree is a maximum likelihood generated with the default settings from MUSCLE. Riboswitches were identified using rfam (66) and by searching the upstream regions of *btuB* and *metE* genes (up to 1,000 bp upstream of their predicted operons).

Proteomap generation. Categories were taken from predefined Kyoto Encyclopedia of Genes and Genomes (KEGG) categories (67). Categories were then ranked based on priority, and any gene that might have been present in more than one category was deleted from those with lower priority. The 200 most numerous proteins were then hand checked. Any that had not been automatically assigned to a KEGG category were compared against other organisms to place them in their most appropriate category. The categorized genes along with the ribosome profiling data were used to create the Proteomap (68).

Strain construction. (i) JS417. The insert btuB_5′UTR was generated by IDT as a gBlock construct for the +1 transcription start site (TSS) through the start codon of the *btuB* gene. The btuB_5′UTR gBlock had the sequence AAGCGTTCAATTGGATCCAATCTTGACGTCCGTTTGATTACGATCAAGATTGGATCCAGCGT CAGGTTCCTCGAAAGAGGATGAAAAGGGAACGAGGTTGAAGACCTCGGCTGCCCCCGCAACTGTAAGCGGCGA GCTTCGCGTCACATGCCACTGGGCCCAAAAGGCCTGGGAAGGCGACGCCCAGAAGCATTGACCCGTGAGCCAG GAGACCTGCCCGGCGCAGTCGTTCATCGCTCGGCCGGGGTGCGCCGAACGAACGGGATCTCCCGAGAAACGAC AGTCAACAGGCCGCGCGACGGCCTGAGCGTCCGCGTCTTCGCGGGCGGTCGGGAGGTCGCGTGGGTCGTTCAT AACGGGAAGACTGTATTATGTTAATTAATATGCATGGTAC.

The plasmid pRVChyC-2 (60) was cut with MfeI and PacI, and the gBlock segment btuB_5′UTR was inserted into the plasmid by Gibson assembly. Next, the resulting plasmid was transformed into *E. coli* DH5α cells and selected on LB-kanamycin (Kan) plates. The resulting Kan^r colonies were then screened by PCR for the insert and verified by Sanger sequencing (Genewiz). The purified plasmid was then transformed into NA1000 cells by electroporation and plated on PYE-Kan plates. The resulting colonies were screened for mChy fluorescence after induction with vanillate.

(ii) JS423. The insert metE_5′UTR was generated by IDT as a gBlock construct for the +1 TSS through the start codon of *metE*. The metE_5′UTR gBlock had the sequence AAGCGTTCAATTGGATCCAATCTTGA CGTCCGTTTGATTACGATCAAGATTGGATCCAGTCGTGGTCTGCGGACGTTCGCGTCCGGAGCTAAGAGGGAAG TCGGTGAGGGCGTGAAACCCTGAATCCGGCGCTGCCCCCGCAACTGTGAGCGGCGAGCCGCTGTCCGTTTCGTG TCACTGACGCGCCGAAGCTGGTTCGGGGATGCGTCGGGAAGGCCAGGGCAGGGGTGACGACCCGTGAGCCAG GAGACCTGCCTCGACAGATAACGTCCTCCGGCGGGGTGTCCGGTCTGGCCGCTTGCTCAGCGCGACCGGACAA

AAGCGCCCGTGCGCGCTCGACCGCGCGCGTCCCGATCAGCCTCGCCAAAACACCGGCAGAGGCTTTTCAAAG ATG TTAATTAATATGCATGGTAC.

The plasmid pRVChyC-6 (60) was cut with MfeI and PacI, and the gBlock segment *metE*_5′UTR was inserted into the plasmid by Gibson assembly. Next, the resulting plasmid was transformed into *E. coli* DH5α cells and selected on LB-chloramphenicol (Chlor) plates. The resulting Chlor^r colonies were then screened by PCR for the insert and verified by Sanger sequencing (Genewiz). The purified plasmid was then transformed into NA1000 cells by electroporation and plated on PYE-Chlor plates. The resulting colonies were screened for mChy fluorescence after induction with vanillate.

(iii) JS440. The plasmid pRVMCS-2 (Kan^r) (60) was transformed into NA1000 cells via electroporation and selected for on PYE-Kan plates.

(iv) JS441. The JS441 strain was generated by PCR amplifying the last 500 bp of the β′ RNA polymerase gene into the pYFPC-1 plasmid (60). The insert was PCR amplified from the NA1000 chromosome using Betaprime_forward and Betaprime_reverse primers, and the plasmid pYFPC-1 (60) was PCR amplified by pYFPC_forward and pYFPC_reverse primers. The plasmid was then treated with restriction enzyme DpnI, and the insert was placed into the plasmid by Gibson assembly. Next, the resulting plasmid was transformed into *E. coli* DH5α cells and selected on LB-spectinomycin (Spec) plates. The resulting Spec^r colonies were then screened by colony PCR for the insert and verified by Sanger sequencing (Genewiz). The purified plasmid was then transformed into NA1000 cells by electroporation and plated on PYE-Spec-streptomycin (Strep) plates. The resulting colonies were screened for YFP fluorescence.

PCR primers were as follows: Betaprime_forward, 5′TAATATGCATGGTGTCGACGAGATCCAGGAGG; Betaprime_reverse, 5′-TCTTAAGGTTTCGGCGTCCGAAAGCGC; pYFPC_forward, 5′-GCTTTCGGACGCCGAAA CCTTAAGATCTCGAGCTCCG; pYFPC_reverse, 5′-GGATCTCGTCGACACCATGCATATTAATTAAGGCGCC.

Data availability. All ribosome profiling raw sequencing reads and normalized read count values of cells grown in M2G are deposited in the NCBI GEO database with accession number GSE126485. PYE ribosome profiling data were collected in reference 36 and were pulled from NCBI GEO database accession number GSE54883. Absolute quantitation values of mRNA translation for both M2G and PYE can be found in Table S1. Ribosome profiling data were compared to the following data sets collected in previous reports. Protein localization data are from reference 26. Tn-seq fitness data are from references 39 and 57. Gene essentiality data are from reference 69. KEGG categories are from reference 70. DNA binding site counts for cell cycle master regulators are from reference 10.

SUPPLEMENTAL MATERIAL

Supplemental material for this article may be found at https://doi.org/10.1128/mSystems.00170-19.

FIG S1, TIF file, 0.8 MB.
FIG S2, TIF file, 2.8 MB.
FIG S3, TIF file, 0.7 MB.
TABLE S1, XLSX file, 0.9 MB.
TABLE S2, DOCX file, 0.01 MB.
TABLE S3, DOCX file, 0.01 MB.
TABLE S4, DOCX file, 0.02 MB.
TABLE S5, DOCX file, 0.01 MB.
TABLE S6, DOCX file, 0.02 MB.
TABLE S7, DOCX file, 0.01 MB.

ACKNOWLEDGMENTS

REFERENCES

1. Hui S, Silverman JM, Chen SS, Erickson DW, Basan M, Wang J, Hwa T, Williamson JR. 2015. Quantitative proteomic analysis reveals a simple strategy of global resource allocation in bacteria. Mol Syst Biol 11:784. https://doi.org/10.15252/msb.20145697.

2. Li GW, Burkhardt D, Gross C, Weissman JS. 2014. Quantifying absolute protein synthesis rates reveals principles underlying allocation of cellular resources. Cell 157:624–635. https://doi.org/10.1016/j.cell.2014.02.033.

3. Bremer H, Dennis PP. 2008. Modulation of chemical composition and other parameters of the cell at different exponential growth rates. EcoSal Plus 3(1). https://doi.org/10.1128/ecosal.5.2.3.

4. Scott M, Klumpp S, Mateescu EM, Hwa T. 2014. Emergence of robust growth laws from optimal regulation of ribosome synthesis. Mol Syst Biol 10:747. https://doi.org/10.15252/msb.20145379.

5. Lalanne JB, Taggart JC, Guo MS, Herzel L, Schieler A, Li GW. 2018. Evolutionary convergence of pathway-specific enzyme expression stoichiometry. Cell 173:749–761.e38. https://doi.org/10.1016/j.cell.2018.03.007.

6. Lasker K, Mann TH, Shapiro L. 2016. An intracellular compass spatially coordinates cell cycle modules in Caulobacter crescentus. Curr Opin Microbiol 33:131–139. https://doi.org/10.1016/j.mib.2016.06.007.

7. Collier J. 2016. Cell cycle control in Alphaproteobacteria. Curr Opin Microbiol 30:107–113. https://doi.org/10.1016/j.mib.2016.01.010.

8. Schrader JM, Li GW, Childers WS, Perez AM, Weissman JS, Shapiro L, McAdams HH. 2016. Dynamic translation regulation in Caulobacter cell cycle control. Proc Natl Acad Sci U S A 113:E6859–E6867. https://doi.org/10.1073/pnas.1614795113.

9. Laub MT, McAdams HH, Feldblyum T, Fraser CM, Shapiro L. 2000. Global analysis of the genetic network controlling a bacterial cell cycle. Science 290:2144–2148. https://doi.org/10.1126/science.290.5499.2144.

10. Zhou B, Schrader JM, Kalogeraki VS, Abeliuk E, Dinh CB, Pham JQ, Cui ZZ, Dill DL, McAdams HH, Shapiro L. 2015. The global regulatory architecture of transcription during the *Caulobacter* cell cycle. PLoS Genet 11:e1004831. https://doi.org/10.1371/journal.pgen.1004831.

11. Berge M, Viollier PH. 2018. End-in-sight: cell polarization by the poly-gamic organizer PopZ. Trends Microbiol 26:363–375. https://doi.org/10.1016/j.tim.2017.11.007.

12. Poindexter JS. 1964. Biological properties and classification of the Cau-lobacter group. Bacteriol Rev 28:231.

13. Oh E, Becker AH, Sandikci A, Huber D, Chaba R, Gloge F, Nichols RJ, Typas A, Gross CA, Kramer G, Weissman JS, Bukau B. 2011. Selective ribosome profiling reveals the cotranslational chaperone action of trigger factor in vivo. Cell 147:1295–1308. https://doi.org/10.1016/j.cell.2011.10.044.

14. Ingolia NT, Ghaemmaghami S, Newman JRS, Weissman JS. 2009. Genome-wide analysis in vivo of translation with nucleotide resolution using ribosome profiling. Science 324:218–223. https://doi.org/10.1126/science.1168978.

15. Grunenfelder B, Rummel G, Vohradsky J, Roder D, Langen H, Jenal U. 2001. Proteomic analysis of the bacterial cell cycle. Proc Natl Acad Sci U S A 98:4681–4686. https://doi.org/10.1073/pnas.071538098.

16. Aretakis JR, Al-Husini N, Schrader JM. 2018. Methodology for ribosome profiling of key stages of the Caulobacter crescentus cell cycle. Methods Enzymol 612:443–465. https://doi.org/10.1016/bs.mie.2018.07.008.

17. Kelly AJ, Sackett MJ, Din N, Quardokus E, Brun YV. 1998. Cell cycle-dependent transcriptional and proteolytic regulation of FtsZ in Caulo-bacter. Genes Dev 12:880–893. https://doi.org/10.1101/gad.12.6.880.

18. Wright R, Stephens C, Zweiger G, Shapiro L, Alley MR. 1996. Caulobacter Lon protease has a critical role in cell-cycle control of DNA methylation. Genes Dev 10:1532–1542. https://doi.org/10.1101/gad.10.12.1532.

19. Jonas K, Liu J, Chien P, Laub MT. 2013. Proteotoxic stress induces a cell-cycle arrest by stimulating Lon to degrade the replication initiator DnaA. Cell 154:623–636. https://doi.org/10.1016/j.cell.2013.06.034.

20. Garcia-Bayona L, Guo MS, Laub MT. 2017. Contact-dependent killing by Caulobacter crescentus via cell surface-associated, glycine zipper pro-teins. Elife 6:e24869. https://doi.org/10.7554/eLife.24869.

21. Berdis AJ, Lee I, Coward JK, Stephens C, Wright R, Shapiro L, Benkovic SJ. 1998. A cell cycle-regulated adenine DNA methyltransferase from Cau-lobacter crescentus processively methylates GANTC sites on hemimethy-lated DNA. Proc Natl Acad Sci U S A 95:2874–2879. https://doi.org/10.1073/pnas.95.6.2874.

22. Spencer W, Siam R, Ouimet MC, Bastedo DP, Marczynski GT. 2009. CtrA, a global response regulator, uses a distinct second category of weak DNA binding sites for cell cycle transcription control in Caulobacter crescentus. J Bacteriol 191:5458–5470. https://doi.org/10.1128/JB.00355-09.

23. Judd EM, Ryan KR, Moerner WE, Shapiro L, McAdams HH. 2003. Fluores-cence bleaching reveals asymmetric compartment formation prior to cell division in Caulobacter. Proc Natl Acad Sci U S A 100:8235–8240. https://doi.org/10.1073/pnas.1433105100.

24. Haakonsen DL, Yuan AH, Laub MT. 2015. The bacterial cell cycle regu-lator GcrA is a sigma70 cofactor that drives gene expression from a subset of methylated promoters. Genes Dev 29:2272–2286. https://doi.org/10.1101/gad.270660.115.

25. Wu X, Haakonsen DL, Sanderlin AG, Liu YJ, Shen L, Zhuang N, Laub MT, Zhang Y. 2018. Structural insights into the unique mechanism of tran-scription activation by Caulobacter crescentus GcrA. Nucleic Acids Res 46:3245–3256. https://doi.org/10.1093/nar/gky161.

26. Werner JN, Chen EY, Guberman JM, Zippilli AR, Irgon JJ, Gitai Z. 2009. Quantitative genome-scale analysis of protein localization in an asym-metric bacterium. Proc Natl Acad Sci U S A 106:7858–7863. https://doi.org/10.1073/pnas.0901781106.

27. Holmes JA, Follett SE, Wang H, Meadows CP, Varga K, Bowman GR. 2016.

Caulobacter PopZ forms an intrinsically disordered hub in organizing bacterial cell poles. Proc Natl Acad Sci U S A 113:12490–12495. https://doi.org/10.1073/pnas.1602380113.

28. Berge M, Campagne S, Mignolet J, Holden S, Theraulaz L, Manley S, Allain FH, Viollier PH. 2016. Modularity and determinants of a (bi-)-polarization control system from free-living and obligate intracellular bacteria. Elife 5:e20640. https://doi.org/10.7554/eLife.20640.

29. Zhao W, Duvall SW, Kowallis KA, Tomares DT, Petitjean HN, Childers WS. 2018. A circuit of protein-protein regulatory interactions enables polarity establishment in a bacterium. bioRxiv https://doi.org/10.1101/503250:503250.

30. Lau JH, Nomellini JF, Smit J. 2010. Analysis of high-level S-layer protein secretion in Caulobacter crescentus. Can J Microbiol 56:501–514. https://doi.org/10.1139/w10-036.

31. Krab IM, Parmeggiani A. 1998. EF-Tu, a GTPase odyssey. Biochim Biophys Acta 1443:1–22. https://doi.org/10.1016/S0167-4781(98)00169-9.

32. Zhang Y, Rodionov DA, Gelfand MS, Gladyshev VN. 2009. Comparative genomic analyses of nickel, cobalt and vitamin B12 utilization. BMC Genomics 10:78. https://doi.org/10.1186/1471-2164-10-78.

33. Menikpurage IP, Barraza D, Melendez AB, Strebe S, Mera PE. 2019. The B12 receptor BtuB alters the membrane integrity of Caulobacter crescentus. Microbiology 165:311–323. https://doi.org/10.1099/mic.0.000753.

34. Whitfield CD, Steers EJ, Jr, Weissbach H. 1970. Purification and properties of 5-methyltetrahydropteroyltriglutamate-homocysteine transmethy-lase. J Biol Chem 245:390–401.

35. Frasca V, Banerjee RV, Dunham WR, Sands RH, Matthews RG. 1988. Cobalamin-dependent methionine synthase from Escherichia coli B: electron paramagnetic resonance spectra of the inactive form and the active methylated form of the enzyme. Biochemistry 27:8458–8465. https://doi.org/10.1021/bi00422a025.

36. Schrader JM, Zhou B, Li GW, Lasker K, Childers WS, Williams B, Long T, Crosson S, McAdams HH, Weissman JS, Shapiro L. 2014. The coding and noncoding architecture of the *Caulobacter crescentus* genome. PLoS Genet 10:e1004463. https://doi.org/10.1371/journal.pgen.1004463.

37. Benoit RJ. 1957. Preliminary observations on cobalt and vitamin B12 in fresh water1. Limnol Oceanogr 2:233–240. https://doi.org/10.1002/lno.1957.2.3.0233.

38. Pommel B. 1975. Distribution et signification écologique de la vitamine B12 et de la thiamine dans trois lacs subalpins et jurassien. Ann Hydro-biol 6:103–121.

39. Price MN, Wetmore KM, Waters RJ, Callaghan M, Ray J, Liu H, Kuehl JV, Melnyk RA, Lamson JS, Suh Y, Carlson HK, Esquivel Z, Sadeeshkumar H, Chakraborty R, Zane GM, Rubin BE, Wall JD, Visel A, Bristow J, Blow MJ, Arkin AP, Deutschbauer AM. 2018. Mutant phenotypes for thousands of bacterial genes of unknown function. Nature 557:503–509. https://doi.org/10.1038/s41586-018-0124-0.

40. Schrader JM, Shapiro L. 2015. Synchronization of Caulobacter crescentus for investigation of the bacterial cell cycle. J Vis Exp (98):e52633. https://doi.org/10.3791/52633:e52633.

41. Ferber DM, Ely B. 1982. Resistance to amino acid inhibition in Caulobac-ter crescentus. Mol Gen Genet 187:446–452. https://doi.org/10.1007/BF00332626.

42. Shen X, Collier J, Dill D, Shapiro L, Horowitz M, McAdams HH. 2008. Architecture and inherent robustness of a bacterial cell-cycle control system. Proc Natl Acad Sci U S A 105:11340–11345. https://doi.org/10.1073/pnas.0805258105.

43. Lin Y, Crosson S, Scherer NF. 2010. Single-gene tuning of Caulobacter cell cycle period and noise, swarming motility, and surface adhesion. Mol Syst Biol 6:445. https://doi.org/10.1038/msb.2010.95.

44. Subramanian K, Tyson JJ. 2017. Spatiotemporal models of the asymmet-ric division cycle of Caulobacter crescentus. Results Probl Cell Differ 61:23–48. https://doi.org/10.1007/978-3-319-53150-2_2.

45. Murray SM, Panis G, Fumeaux C, Viollier PH, Howard M. 2013. Compu-tational and genetic reduction of a cell cycle to its simplest, primordial components. PLoS Biol 11:e1001749. https://doi.org/10.1371/journal.pbio.1001749.

46. Christen M, Deutsch S, Christen B. 2015. Genome Calligrapher: a web tool for refactoring bacterial genome sequences for de novo DNA synthesis. ACS Synth Biol 4:927–934. https://doi.org/10.1021/acssynbio.5b00087.

47. Venetz JE, Del Medico L, Wolfle A, Schachle P, Bucher Y, Appert D, Tschan F, Flores-Tinoco CE, van Kooten M, Guennoun R, Deutsch S, Christen M, Christen B. 2019. Chemical synthesis rewriting of a bacterial

genome to achieve design flexibility and biological functionality. Proc Natl Acad Sci U S A 116:8070–8079. https://doi.org/10.1073/pnas .1818259116.

48. Al-Husini N, Tomares DT, Bitar O, Childers WS, Schrader JM. 2018. Alpha-proteobacterial RNA degradosomes assemble liquid-liquid phase-separated RNP bodies. Mol Cell 71:1027–1039.e14. https://doi.org/10 .1016/j.molcel.2018.08.003.

49. Banani SF, Lee HO, Hyman AA, Rosen MK. 2017. Biomolecular condensates: organizers of cellular biochemistry. Nat Rev Mol Cell Biol 18:285–298. https://doi.org/10.1038/nrm.2017.7.

50. Lasker K, von Diezmann A, Ahrens DG, Mann TH, Moerner WE, Shapiro L. 2018. Phospho-signal flow from a pole-localized microdomain spatially patterns transcription factor activity. bioRxiv https://doi.org/10.1101/ 220293:220293.

51. Childers WS, Xu Q, Mann TH, Mathews II, Blair JA, Deacon AM, Shapiro L. 2014. Cell fate regulation governed by a repurposed bacterial histidine kinase. PLoS Biol 12:e1001979. https://doi.org/10.1371/journal.pbio .1001979.

52. Daisley KW. 1969. Monthly survey of vitamin B12 concentrations in some waters of the English Lake District. Limnol Oceanogr 14:224–228. https://doi.org/10.4319/lo.1969.14.2.0224.

53. Ohwada K, Taga N. 1972. Vitamin B12, thiamine, and biotin in Lake Sagami1. Limnol Oceanogr 17:315–320. https://doi.org/10.4319/lo.1972 .17.2.0315.

54. Ohwada K. 1973. Seasonal cycles of vitamin B12, thiamine and biotin in Lake Sagami. Patterns of their distribution and ecological significance. Int Rev Gesamten Hydrobiol Hydrogr 58:851–871. https://doi.org/10 .1002/iroh.19730580607.

55. Cavari B, Grossowicz N. 1977. Seasonal distribution of vitamin B12 in Lake Kinneret. Appl Environ Microbiol 34:120–124.

56. Ohwada K, Otsuhata M, Taga N. 1972. Seasonal cycles of vitamin-B12, thiamine and biotin in surface water of Lake Tsukui. Bull Jpn Soc Sci Fish 38:817–823. https://doi.org/10.2331/suisan.38.817.

57. Hentchel KL, Reyes Ruiz LM, Curtis PD, Fiebig A, Coleman ML, Crosson S. 2019. Genome-scale fitness profile of Caulobacter crescentus grown in natural freshwater. ISME J 13:523–536. https://doi.org/10.1038/s41396 -018-0295-6.

58. Wilhelm RC. 2018. Following the terrestrial tracks of Caulobacter—redefining the ecology of a reputed aquatic oligotroph. ISME J 12:3025–3037. https://doi.org/10.1038/s41396-018-0257-z.

59. Duda J, Malinska E, Pedziwilk Z. 1957. Relation between the vitamin B12 content and the microorganism count in soil. Acta Microbiol Pol (1952) 6:355–365.

60. Thanbichler M, Iniesta AA, Shapiro L. 2007. A comprehensive set of plasmids for vanillate- and xylose-inducible gene expression in Caulobacter crescentus. Nucleic Acids Res 35:e137. https://doi.org/10.1093/ nar/gkm818.

61. Ingolia NT, Brar GA, Rouskin S, McGeachy AM, Weissman JS. 2012. The ribosome profiling strategy for monitoring translation in vivo by deep sequencing of ribosome-protected mRNA fragments. Nat Protoc 7:1534–1550. https://doi.org/10.1038/nprot.2012.086.

62. Thanbichler M, Shapiro L. 2006. MipZ, a spatial regulator coordinating chromosome segregation with cell division in Caulobacter. Cell 126:147–162. https://doi.org/10.1016/j.cell.2006.05.038.

63. Ducret A, Quardokus EM, Brun YV. 2016. MicrobeJ, a tool for high throughput bacterial cell detection and quantitative analysis. Nat Microbiol 1:16077. https://doi.org/10.1038/nmicrobiol.2016.77.

64. Sayers EW, Agarwala R, Bolton EE, Brister JR, Canese K, Clark K, Connor R, Fiorini N, Funk K, Hefferon T, Holmes JB, Kim S, Kimchi A, Kitts PA, Lathrop S, Lu Z, Madden TL, Marchler-Bauer A, Phan L, Schneider VA, Schoch CL, Pruitt KD, Ostell J. 2019. Database resources of the National Center for Biotechnology Information. Nucleic Acids Res 47:D23–D28. https://doi.org/10.1093/nar/gky1069.

65. Edgar RC. 2004. MUSCLE: multiple sequence alignment with high accuracy and high throughput. Nucleic Acids Res 32:1792–1797. https://doi .org/10.1093/nar/gkh340.

66. Gardner PP, Daub J, Tate J, Moore BL, Osuch IH, Griffiths-Jones S, Finn RD, Nawrocki EP, Kolbe DL, Eddy SR, Bateman A. 2011. Rfam: Wikipedia, clans and the "decimal" release. Nucleic Acids Res 39:D141–D145. https://doi.org/10.1093/nar/gkq1129.

67. Kanehisa M, Goto S. 2000. KEGG: Kyoto encyclopedia of genes and genomes. Nucleic Acids Res 28:27–30. https://doi.org/10.1093/nar/28.1 .27.

68. Liebermeister W, Noor E, Flamholz A, Davidi D, Bernhardt J, Milo R. 2014. Visual account of protein investment in cellular functions. Proc Natl Acad Sci U S A 111:8488–8493. https://doi.org/10.1073/pnas.1314810111.

69. Christen B, Abeliuk E, Collier JM, Kalogeraki VS, Passarelli B, Coller JA, Fero MJ, McAdams HH, Shapiro L. 2011. The essential genome of a bacterium. Mol Syst Biol 7:528. https://doi.org/10.1038/msb.2011.58.

70. Kanehisa M, Goto S, Sato Y, Kawashima M, Furumichi M, Tanabe M. 2014. Data, information, knowledge and principle: back to metabolism in KEGG. Nucleic Acids Res 42:D199–D205. https://doi.org/10.1093/nar/ gkt1076.

71. Taylor JA, Ouimet MC, Wargachuk R, Marczynski GT. 2011. The Caulobacter crescentus chromosome replication origin evolved two classes of weak DnaA binding sites. Mol Microbiol 82:312–326. https://doi.org/10 .1111/j.1365-2958.2011.07785.x.

72. Fioravanti A, Fumeaux C, Mohapatra SS, Bompard C, Brilli M, Frandi A, Castric V, Villeret V, Viollier PH, Biondi EG. 2013. DNA binding of the cell cycle transcriptional regulator GcrA depends on N6-adenosine methylation in Caulobacter crescentus and other Alphaproteobacteria. PLoS Genet 9:e1003541. https://doi.org/10.1371/journal.pgen.1003541.

73. Fiebig A, Herrou J, Fumeaux C, Radhakrishnan SK, Viollier PH, Crosson S. 2014. A cell cycle and nutritional checkpoint controlling bacterial surface adhesion. PLoS Genet 10:e1004101. https://doi.org/10.1371/ journal.pgen.1004101.

74. Kozdon JB, Melfi MD, Luong K, Clark TA, Boitano M, Wang S, Zhou B, Gonzalez D, Collier J, Turner SW, Korlach J, Shapiro L, McAdams HH. 2013. Global methylation state at base-pair resolution of the Caulobacter genome throughout the cell cycle. Proc Natl Acad Sci U S A 110:E4658–E4667. https://doi.org/10.1073/pnas.1319315110.

75. Fumeaux C, Radhakrishnan SK, Ardissone S, Theraulaz L, Frandi A, Martins D, Nesper J, Abel S, Jenal U, Viollier PH. 2014. Cell cycle transition from S-phase to G1 in Caulobacter is mediated by ancestral virulence regulators. Nat Commun 5:4081. https://doi.org/10.1038/ncomms5081.

76. Evinger M, Agabian N. 1977. Envelope-associated nucleoid from Caulobacter crescentus stalked and swarmer cells. J Bacteriol 132:294–301.

77. Bayas CA, Wang J, Lee MK, Schrader JM, Shapiro L, Moerner WE. 2018. Spatial organization and dynamics of RNase E and ribosomes in Caulobacter crescentus. Proc Natl Acad Sci U S A 115:E3712–E3721. https://doi .org/10.1073/pnas.1721648115.

78. Iniesta AA, Hillson NJ, Shapiro L. 2010. Polar remodeling and histidine kinase activation, which is essential for Caulobacter cell cycle progression, are dependent on DNA replication initiation. J Bacteriol 192:3893–3902. https://doi.org/10.1128/JB.00468-10.

79. Jensen RB, Wang SC, Shapiro L. 2001. A moving DNA replication factory in Caulobacter crescentus. EMBO J 20:4952–4963. https://doi.org/10 .1093/emboj/20.17.4952.

80. Lee SF, Thompson MA, Schwartz MA, Shapiro L, Moerner WE. 2011. Super-resolution imaging of the nucleoid-associated protein HU in Caulobacter crescentus. Biophys J 100:L31–L33. https://doi.org/10.1016/j.bpj .2011.02.022.

81. Jensen RB, Shapiro L. 2003. Cell-cycle-regulated expression and subcellular localization of the Caulobacter crescentus SMC chromosome structural protein. J Bacteriol 185:3068–3075. https://doi.org/10.1128/JB.185 .10.3068-3075.2003.